INTERNATIONAL JOURNAL FOR NUMERICAL METHODS IN FLUIDS
Int. J. Numer. Meth. Fluids 2002; **39**:1161–1178 (DOI: 10.1002/fld.365)

A novel finite point method for flow simulation

M. Cheng*,† and G. R. Liu‡

Institute of High Performance Computing, 89B Science Park Drive #02-11/12, The Rutherford Singapore Science Park I, Singapore 118261, Singapore

SUMMARY

A novel finite point method is developed to simulate flow problems. The mashes in the traditional numerical methods are supplanted by the distribution of points in the calculation domain. A local interpolation based on the properties of Taylor series expansion is used to construct an approximation for unknown functions and their derivatives. An upwind-dominated scheme is proposed to efficiently handle the non-linear convection. Comparison with the finite difference solutions for the two-dimensional driven cavity flow and the experimental results for flow around a cylinder shows that the present method is capable of satisfactorily predicting the flow separation characteristic. The present algorithm is simple and flexible for complex geometric boundary. The influence of the point distribution on computation time and accuracy of results is included. Copyright © 2002 John Wiley & Sons, Ltd.

KEY WORDS: finite point method; Taylor series expansion; mesh-free techniques; computational fluid dynamics; flow separation

1. INTRODUCTION

With the development of modern high-speed computers, a lot of complex problems in computational fluid dynamics, such as the solution of three-dimensional flow in engineering, can be simulated using the traditional finite element and finite volume methods when an acceptable mesh is provided. The generation of meshes, however, can spend far more time and cost than the numerical solution itself in many cases of industrial computation. Therefore, the mesh generation remains one of the big challenges for modelling complicated boundary conditions and multiphase interfaces of arbitrary shape. In recent years, the mesh free method or the finite point method has attracted much attention in computational mechanics.

A lot of effort has been devoted to the development of the mesh-free schemes in computational mechanics. The earliest attempt to use a local interpolation scheme for an irregular

*Correspondence to: M. Cheng, Institute of High Performance Computing, 89B SciencePark Drive #02-11/12, The Rutherford Singapore Science Park I, 118261 Singapore, Singapore.
†E-mail: chengm@ihpc.nus.edu.sg
‡E-mail: mpeliugr@nus.edu.sg

Received July 1999
Revised July 2001

mesh of nodal points in the finite difference method (FDM) was made by Perrone and Kao in 1975 [1] to solve a Poisson equation and a flat membrane problem. In their scheme, the domain in the vicinity of a given central point is divided into eight 45° pies shaped segments and the closest finite difference point in each segment is selected. Taylor series expansions about the central point and an averaging process on the four points in the diagonal segments are used to construct an approximation for derivatives up to the second order. When applied to square meshes, these general derivative expressions for arbitrary meshes reduce to the usual finite difference formulae. A local interpolation method, which is based on a Taylor expansion of the unknown function combined with the minimization of errors, was proposed by Liszka and Orkisz in 1980 [2, 3]. By the appropriate definition of weighting coefficients, this method may be viewed as an interpolation or approximation in the sense of minimum deviation from given values.

An alternative method, smoothed particle hydrodynamics method, which uses no underlying grid, was first introduced by Gingold and Mongghan in 1977 [4]. This method is now being used for a wide variety of impact problems [5, 6]. More recently, an element-free Galerkin method, which is applicable to elasticity and heat conduction problems, has been proposed by Belytschko *et al.* [7] in 1994. In this method, moving least-squares interpolation is used to construct the trial and test functions for the variational principle. Their study results showed that the rate of convergence can exceed that of finite elements significantly and a high resolution of localized steep gradients can be achieved. Liu *et al.* [8, 9] have developed a different class of gridless multiple-scale methods based on reproducing kernel and wavelet analysis. This technique termed Reproducing Kernel Particle method allows one to develop a new type of shape functions using an integral window transform. The window function can be translated and dilated around the domain thus replacing the need to define elements and providing refinement.

Presently, a penalty method for enforcing essential boundary conditions in element-free Galerkin method is proposed by Liu and Yang [10]. They found that the system equation produced using penalty method has the same size as that produced by conventional finite element method for boundary value problems of both homogeneous and inhomogeneous material, and can be much smaller than the size of that produced using Lagrange multipliers in the element-free Galerkin formulation. The method has also been applied for problems with essential boundaries and material discontinuity. Some other types of mesh free techniques have also been reported [10–12].

An excellent review, covering most aspects of this subject in great detail, has been written by Onate *et al.* [13] and Duarte [14].

A thorough literature survey reveals, however, that there is relatively little scheme applied to flow problem, especially, for high Reynolds numbers flow. The purpose of the present paper is to develop a finite point method (FPM) for flow analysis. In the present scheme, mashes are supplanted by the distribution of points in the calculation domain. The discretization of the unknown function and its derivatives are defined only by the position of the points. The unknown function at a point is approximated by an interpolation function, which is based on the properties of Taylor expansions. This new scheme can provide great flexibility and convenience in the implementation of boundary conditions and coding.

2. FINITE POINT METHOD

2.1. Numerical procedure

Consider the equation

$$D\left(x, y, f, \frac{\partial f}{\partial x}, \frac{\partial f}{\partial y}, \frac{\partial f^2}{\partial x \partial y}, \frac{\partial f^2}{\partial x^2}, \frac{\partial f^2}{\partial y^2}, \ldots\right) = g(x, y), \quad (x, y) \in \Omega \tag{1}$$

with

$$f(x, y) = h(x, y), \quad (x, y) \in \Gamma \tag{2}$$

where D is the appropriate physics governing equation, $f(x, y)$ is the unknown, $g(x, y)$ is sources acting over the domain Ω, and $h(x, y)$ is the prescribed value of $f(x, y)$ over the domain's boundary Γ. $f(x, y)$ at the point $P_0(x_0, y_0)$ in the domain can be expressed in terms of the values of $f(x, y)$ at nearby points. For any sufficiently differentiable function $f(x, y)$ in a given domain the Taylor series expansion around a point $P_0(x_0, y_0)$ can be used

$$f_i = f_0 + \sum_{m=1}^{M} \frac{1}{n!} \left(\Delta x \frac{\partial}{\partial x} + \Delta y \frac{\partial}{\partial y}\right)^m f_0 + O(\varepsilon^{M+1}) \tag{3}$$

where

$$f_i = f(x, y), \quad f_0 = f(x_0, y_0), \quad \Delta x = x - x_0, \quad \Delta y = y - y_0, \quad \varepsilon = \sqrt{\Delta x^2 + \Delta y^2}$$

Writing Equation (3) for the M points around the point $P_0(x_0, y_0)$, one can derive the linear systems of equations of the form

$$\mathbf{AW} = \mathbf{F} \tag{4}$$

where

$$\boldsymbol{A} = \begin{bmatrix} \Delta x_1 & \Delta y_1 & \Delta x_1 \Delta y_1 & \frac{1}{2}\Delta x_1^2 & \frac{1}{2}\Delta y_1^2 & \cdots \\ \Delta x_2 & \Delta y_2 & \Delta x_2 \Delta y_2 & \frac{1}{2}\Delta x_2^2 & \frac{1}{2}\Delta y_2^2 & \cdots \\ \Delta x_3 & \Delta y_3 & \Delta x_3 \Delta y_3 & \frac{1}{2}\Delta x_3^2 & \frac{1}{2}\Delta y_3^2 & \cdots \\ \vdots & \vdots & \vdots & \vdots & \vdots & \cdots \\ \Delta x_M & \Delta y_M & \Delta x_M \Delta y_M & \frac{1}{2}\Delta x_M^2 & \frac{1}{2}\Delta y_M^2 & \cdots \end{bmatrix}$$

$$\boldsymbol{W}^{\mathrm{T}} = \left[\frac{\partial f_0}{\partial x}, \frac{\partial f_0}{\partial y}, \frac{\partial f_0^2}{\partial x \partial y}, \frac{\partial f_0^2}{\partial x^2}, \frac{\partial f_0^2}{\partial y^2} \cdots\right]$$

$$\boldsymbol{F}^T = [f_1 - f_0, f_2 - f_0, f_3 - f_0, \ldots, f_M - f_0]$$

If the matrix $\boldsymbol{A}$ is non-singular, then the solution of Equation (4) is

$$\mathbf{W} = \mathbf{A}^{-1}\mathbf{F} \tag{5}$$

By substituting (5) into (1), the relation of f_0 with f_j $(i=1,2,3,\ldots,M)$ can be written formally as

$$\Theta(f_1,f_2,f_3,\ldots,f_M)+f_0\Pi(\Delta x_1,\Delta x_2,\Delta x_3,\ldots,\Delta x_M,\Delta y_1,\Delta y_2,\Delta y_3,\ldots,\Delta y_M)=g \tag{6}$$

therefore,

$$f_0=\frac{\Theta(f_1,f_2,f_3,\ldots,f_M)-g}{\Pi(\Delta x_1,\Delta x_2,\Delta x_3,\ldots,\Delta x_M,\Delta y_1,\Delta y_2,\Delta y_3,\ldots,\Delta y_M)} \tag{7}$$

For Dirichlet boundary condition (2), solution of Equation (1) in domain Ω can be obtained using the SOR method. When Neumann boundary condition is specified on the domain boundary Γ,

$$B\left(x,y,\frac{\partial f}{\partial x},\frac{\partial f}{\partial y},\frac{\partial f^2}{\partial x\partial y},\frac{\partial f^2}{\partial x^2},\frac{\partial f^2}{\partial y^2},\cdots\right)=h' \tag{8}$$

an equation, which is the same as Equation (7) in form, can be derived for f_B subject to Equation (8), i.e.

$$f_B=\frac{\Theta'(f_1,f_2,f_3,\ldots,f_N)-h'}{\Pi'(\Delta x_1,\Delta x_2,\Delta x_3,\ldots,\Delta x_N,\Delta y_1,\Delta y_2,\Delta y_3,\ldots,\Delta y_N)} \tag{9}$$

where N is the number of points around the point $P_B(x_B,y_B)$ on the boundary Γ. The solution of Equation (1) in domain Ω can be obtained by iterating Equations (7) and (8).

2.2. Six-point scheme

For two-dimensional flow problem, five points at the least are selected to determine f_0 because the Navier–Stokes equations are the second-order partial differential equations. As reported by Liszka and Orkisz [2], the main difficulty in a successful application of the finite point approach is to avoid singular or an ill-conditioned matrix $\boldsymbol{A}$ so as to obtain acceptable derivatives $\boldsymbol{W}$. Therefore, it is important to select the points from the domain around a given point in order to avoid the singular. On the other hand, as is well known, fluid flow consists of two mechanisms of diffusion and convection, which occur simultaneously. It is also important to approximate properly the convection term in the Navier–Stokes equations in order to obtain better solutions of flow problems at high Reynolds numbers. In this paper, a 6-point scheme is proposed. More specifically, the sub-domain around the central point $P_0(x_0,y_0)$ is divided into eight equal regions, I–VIII (see Figure 1(a)). The point, which is the nearest from the central point, is selected every two regions. Points 1–4 is selected from regions I, III, V and VII. The 5th point is selected according to the flow direction at the point $P_0(x_0,y_0)$, as shown in Figures 1(a) and 1(b). For example, when $u\geqslant 0$ and $v\geqslant 0$ at the central point $P_0(x_0,y_0)$, point 5 is selected from regions VI, when $u\leqslant 0$ and $v\leqslant 0$ at the central point $P_0(x_0,y_0)$, point 5 is selected from regions II. It should be noted that in the present scheme, it is essential to find the inverse $\boldsymbol{A}^{-1}$ of a 6×6 matrix $\boldsymbol{A}$ at every computing points. The more the number of points, the more time it will take to compute the inverse of matrix. However, once the point distribution is given, the $\boldsymbol{A}$ or $\boldsymbol{A}^{-1}$ can be determined, thus, before performing numerical iteration, one will only calculate the inverse $\boldsymbol{A}^{-1}$ of matrix $\boldsymbol{A}$ once at every points.

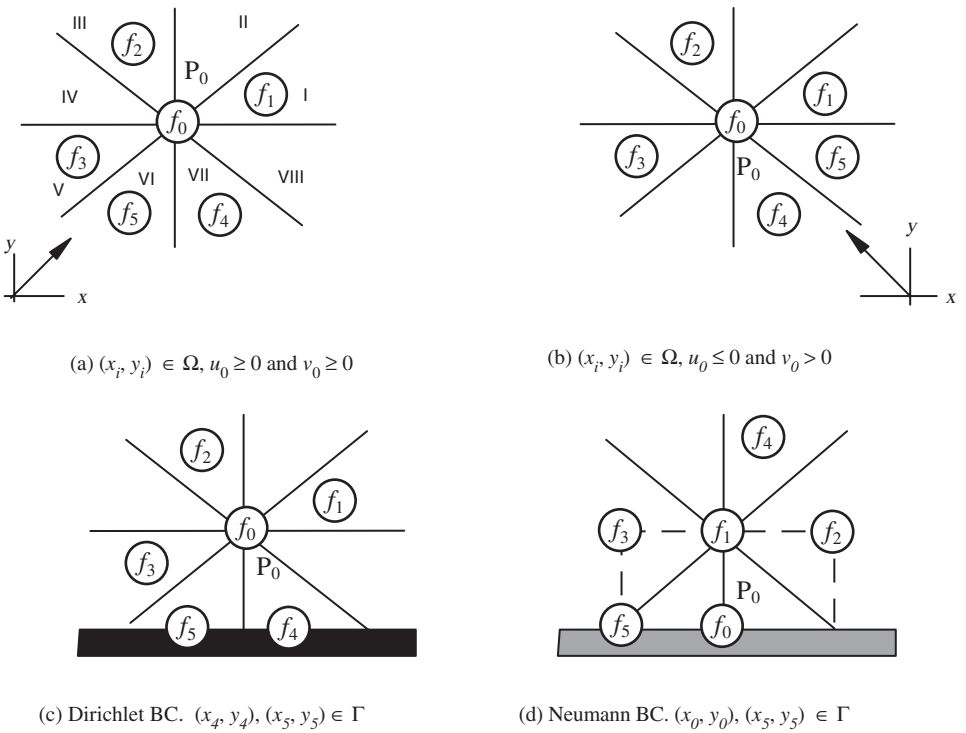

(a) $(x_i, y_i) \in \Omega$, $u_0 \geq 0$ and $v_0 \geq 0$

(b) $(x_i, y_i) \in \Omega$, $u_0 \leq 0$ and $v_0 > 0$

(c) Dirichlet BC. $(x_4, y_4), (x_5, y_5) \in \Gamma$

(d) Neumann BC. $(x_0, y_0), (x_5, y_5) \in \Gamma$

Figure 1. Six-point scheme.

For Dirichlet boundary condition, the central point $P_0(x_0, y_0)$ always locates in domain Ω because f_b is known on the boundary Γ. Thus, the way of the selecting point is the same as mentioned above near the boundary (see Figure 1(c)). When Neumann boundary condition is specified on the domain boundary Γ, on the account of accuracy consideration, parallel points distribution is used. One layer lies on the boundary and another is in the domain. This is because that this distribution is simple, and convenient to apply the 6-point scheme (see Figure 1(d)).

In order to analyse the upwind property of the present numerical scheme, we will illustrate them on a typical convection equation, written here as follows:

$$uf_x + vf_y = 0 \tag{10}$$

where u and v are the convection speed.

For convenience, assume that the point coincides with the node of a rectangular mesh, and the velocity u and v are positive constants, respectively, as shown in Figure 2. When $M = 6$, Equation (5) can be written as

$$f_x = \frac{f_1 - f_3}{2\Delta x} \tag{11}$$

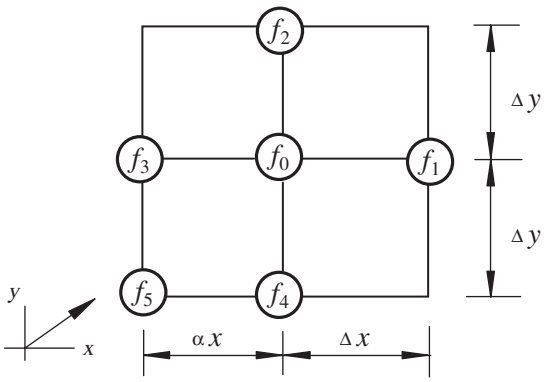

Figure 2. Rectangular mesh.

$$f_y = \frac{f_2 - f_4}{2\Delta y} \tag{12}$$

$$f_{xy} = \frac{f_5 + f_0 - f_3 - f_4}{\Delta x \Delta y} \tag{13}$$

$$f_{xx} = \frac{f_1 - 2f_0 + f_3}{\Delta x^2} \tag{14}$$

$$f_{yy} = \frac{f_2 - 2f_0 + f_4}{\Delta y^2} \tag{15}$$

Substituting (11) and (12) into (10) gives

$$\frac{u}{2\Delta x}(f_1 - f_3) + \frac{v}{2\Delta y}(f_2 - f_4) = 0 \tag{16}$$

In order to get f_0 the second-order equation can be derived from Equation (10) by differentiating it with respect to x and y, respectively.

$$uf_{xx} + vf_{xy} = uf_{xy} + vf_{yy} = 0 \tag{17}$$

Similarly, by substituting (13), (14) and (15) into (17), the value of f_0 can then been written as

$$f_0 = \left[\frac{u+v}{\Delta x \Delta y}(f_5 - f_3 - f_4) + \frac{u}{\Delta x^2}(f_1 + f_3) + \frac{v}{\Delta y^2}(f_2 + f_4)\right] \Big/ \left(\frac{2u}{\Delta x^2} + \frac{2v}{\Delta y^2} - \frac{u+v}{\Delta x \Delta y}\right) \tag{18}$$

Setting $\Delta x = \Delta y$ and taking into account (16), one obtains

$$f_0 = f_5 + \frac{u - v}{u + v}(f_3 - f_4) \tag{19}$$

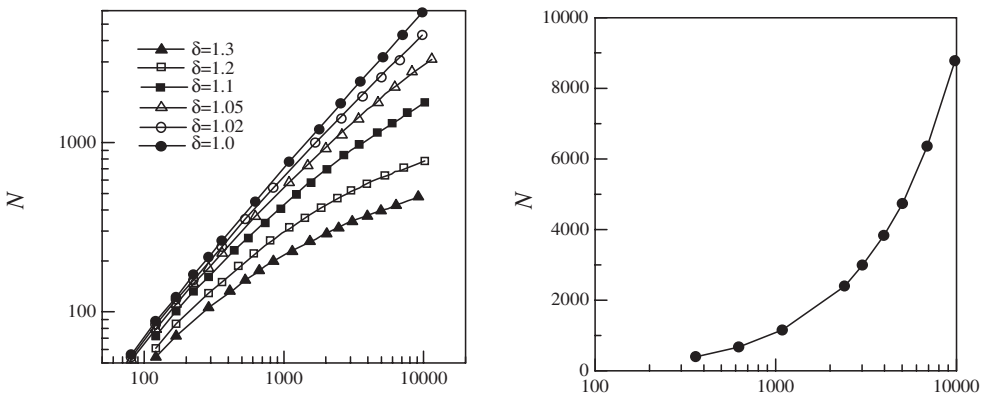

(a) Structured points (b) Unstructured points

Figure 3. The number of iterations required to satisfy the convergence criterion for different number of points.

It is clear that f_0 is determined by f_3, f_4 and f_5 at upwind position, and when $u=v$, $f_0=f_5$. The present scheme not only avoids the singularity in the derivative coefficient matrix $\boldsymbol{A}$ in which rows or columns of the matrix are linearly connected by certain relations, but also forms a structure of upwind points domination; hence, it greatly increase the stability of schemes. Even though the function $f(x, y)$ expressions for arbitrary meshes reduce to the usual finite difference formulae when applied to square meshes, the present scheme possesses both the accuracy of the second-order central difference and characteristic of upwind domination.

2.3. *Effect of point distribution density*

In order to discuss the influence of the point distribution density on time and accuracy of computation, let us consider the Laplace's equation

$$f_{xx} + f_{yy} = 0 \tag{20}$$

which governs incompressible, potential flow. It is a typical elliptic equation, describing an isotropic diffusion in the (x, y) space.

For boundary conditions

$$f(x,0) = \sin(\pi x), \quad f(x,1) = \sin(\pi x)\exp(-\pi), \quad f(0,y) = f(1,y) = 0 \tag{21}$$

Equation (18) has the exact solution

$$f(x,y) = \sin(\pi x)\exp(-\pi y) \tag{22}$$

The influence of the number of points on the computation time is checked for both structured (the point coincides with the node of a rectangular mesh, see Figures 5(a) and 5(b)) and unstructured points distribution (see Figures 5(c) and 5(d)). Figure 3 illustrates the number of iterations required to satisfy the convergence criterion for different number of points. The

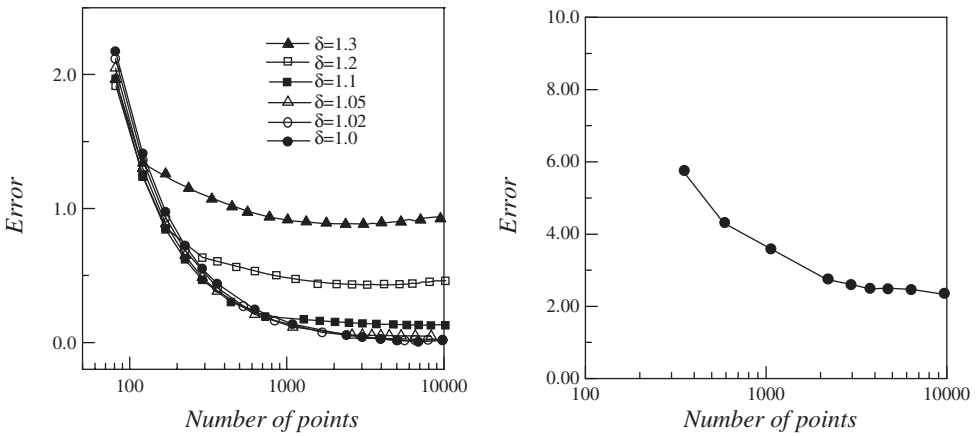

(a) Structured points (b) Unstructured points

Figure 4. Relative error when the iteration satisfies the convergence criterion for different number of points.

iteration is terminated when values of the dependent variable at each point satisfy the following convergence criterion:

$$|f_j^n - f_j^{n-1}| \leqslant 10^{-7} \tag{23}$$

where f_j stands for any dependent variable, and n is the iteration level. As might be expected, the computer time grows with the number of points. This can be seen from Figure 3 that the number of iterations required attaining a given accuracy with SOR increases with the increase of the number of points. In the case of structured points distribution, for a given number of points, the number of iterations required to satisfy the convergence criterion decreases with the increase of δ (where δ is the ratio of the distances from the centre point to the farthest and nearest points in the 6-point scheme). This is because that the density of points near the boundary increases with the increase of δ in the present computation. Furthermore, it is found that the number required to satisfy the convergence criterion is more in the case of unstructured points distribution than in the case of structured points distribution at the same number of points. Usually, a large number of points are required for a complex practical flow problem, but, fortunately, the parallel numerical algorithms have provided an effective and yet very natural way of accelerating the computation for the point iteration processing method. Figure 4 shows the relative error against the number of points when the iteration satisfies the convergence criterion. The errors are calculated according to following formula:

$$\text{Error} = \text{maximum} \frac{|f_j^N - f_j^{\text{exact}}|}{|f_j^{\text{exact}}|} \times 100 \tag{24}$$

where N is the number of iterations required to satisfy the convergence criterion (23) at each point. It is found that the error decreases with the increase of the number of calculation points. However, when the number of points goes beyond 2000 the error approaches an asymptotic value. In the case of structured points distribution, for a given number of points, the error

increases with the increase of δ. When $\delta < 1.1$, the relative error is below 0.5%, when $\delta > 1.1$, the error increases remarkably. It can be explained by the fact that the truncation error ε is proportional to the distance between the farthest point and the centre point in the 6-point scheme. If the point distribution does not vary uniformly a loss of accuracy is unavoidable. This is similar to the property of finite difference approximation on non-uniform meshes. However, if the δ is limited below 1.1 in the 6-point scheme, a satisfactory accuracy can be achieved in practical flow simulation. Further discussion is included in the next section.

3. NUMERICAL SIMULATION AND COMPARISONS

3.1. Shear driven flow in a square cavity

The two-dimensional viscous incompressible flow in a square cavity whose top wall moves with a uniform velocity in its own plane has served as a model problem for testing and evaluating the present numerical scheme because of the complexity of flows.

The flow governing equations in stream function ψ and vorticity ζ formulation are

$$\psi_{xx} + \psi_{yy} = \zeta \tag{25}$$

$$Re\,\zeta_t + Re(\psi_y \zeta_x - \psi_x \zeta_y) = \zeta_{xx} + \zeta_{yy} \tag{26}$$

with boundary conditions

$$\psi(x,0,t) = \psi(x,1,t) = \psi(0,y,t) = \psi(1,y,t) = 0 \tag{27}$$

The vorticity boundary condition is determined from Equation (25). On account of accuracy consideration, parallel points distribution is used. Thus, a second formula is proposed that can be written as

$$\zeta = -\frac{6[\psi(\Delta r,t) + u_B \Delta r] + \zeta(\Delta r,t)\Delta r^2}{2\Delta r^2} \tag{28}$$

where Δr is the distance between the parallel points, u_B is the tangential velocity along the boundary.

An unsteady approach, in which the solution evolves into steady state, is employed in the present work. Furthermore, the implicit scheme is used for the time derivative, and the time step is chosen as 0.005. At each time level the iteration is terminated when values of the dependent variables at each point satisfy the following convergence criterion:

$$|\psi_j^n - \psi_j^{n-1}| \leqslant 10^{-7} \tag{29}$$

and

$$|\zeta_j^n - \zeta_j^{n-1}| \leqslant 10^{-5} \tag{30}$$

It must be pointed out that ψ and ζ shear the same coefficient matrix $\boldsymbol{A}$ at a given point in the domain. Thus, for the solution of Equation (4) a single matrix inversion is required, diminishing the computational time.

Figure 5 shows a comparison of the flow field and streamline patterns for $Re=400$ and different number of points. These plots give a clear picture of the overall flow pattern and the effect of the number of points on the structure of the steady recirculating vortices in the cavity. For structured point distribution, it should be noted that when the number of points is 441 ($\delta=1.3$) the vortices of the left and right lower corners of the cavity, where the point distribution is dense, can been seen. But the streamline value at the centre of the primary vortex, where the points are thinly scattered, is lower than that of solutions by FDM [15]. When the number of points increases from 441 to 2601 ($\delta=1.05$), the calculated streamline pattern and values in full flow field agree better with those solutions obtained by FDM [15]. Figures 5(c) and 5(d) show the results at different number of points for unstructured points distribution. The influence of the number of points on the results is similar to the case of structured points distribution. Better resolution is obtained as the number of point increases. When the point distribution increases to 13 689 the agreement between the results obtained by two methods is quite good. However, it is found that the results by FPM almost remain unchanged even if the number of points is increased further. As discussed earlier, the computation time grows with the increase of the number of points. But for structured points distribution, $\delta<1.1$, when the points are greater than a certain number the error approaches an asymptotic value. The present results show that if one is interested in only global property, such as flow pattern, a relatively coarse point distribution should be adopted. Hence, if the resolution of local properties is also of interest, a finer point distribution will be necessary.

The comparison of the values of streamline and vorticity contours with the numerical results of Ghia *et al.* [15] for $Re=400$ is shown in Figure 6. It can be seen that generally the qualitative agreement between the results obtained by the two methods is good. In addition to the primary, the centre vortex, a pair of counter-rotating vortices with much smaller strength develops in the lower corners of the cavity. It is found that the primary vortex centre is at $x=0.555$ and $y=0.608$ when $Re=400$. The location of the vortex centre predicted by FPM is in close agreement with $x=0.5547$ and $y=0.6055$, reported by Ghia *et al.* [15] and $x=0.5608$ and $y=0.6078$ obtained by Chen *et al.* [16] at the same Reynolds number.

Figure 7 shows the velocity profiles through the geometric centre of cavity for structured points distribution. It is found that the use of 441 points is not adequate to accurately predict the flow. The use of 2601 points, however, yields results that are in good agreement with the results reported in Reference [15] at the same Reynolds number. This figure clearly indicates that as the number of points increases, the accuracy increases.

3.2. Flow past a circular cylinder

In order to further illustrate the usefulness and accuracy of the present method, flow around an impulsively started circular cylinder was computed for irregular point distribution. The number of points are 20 100 and $\delta=1.05$, as shown in Figure 8. Here Equations (25) and (26) were solved together with the boundary conditions: no slip condition on the surface of the cylinder; potential flow at infinity. These conditions can be written in stream function and vorticity formulation as

$$\psi=0, \quad \zeta=-\frac{6\psi(\Delta r,t)+\zeta(\Delta r,t)\Delta r^2}{2\Delta r^2} \quad \text{on } \Gamma_1 \tag{31}$$

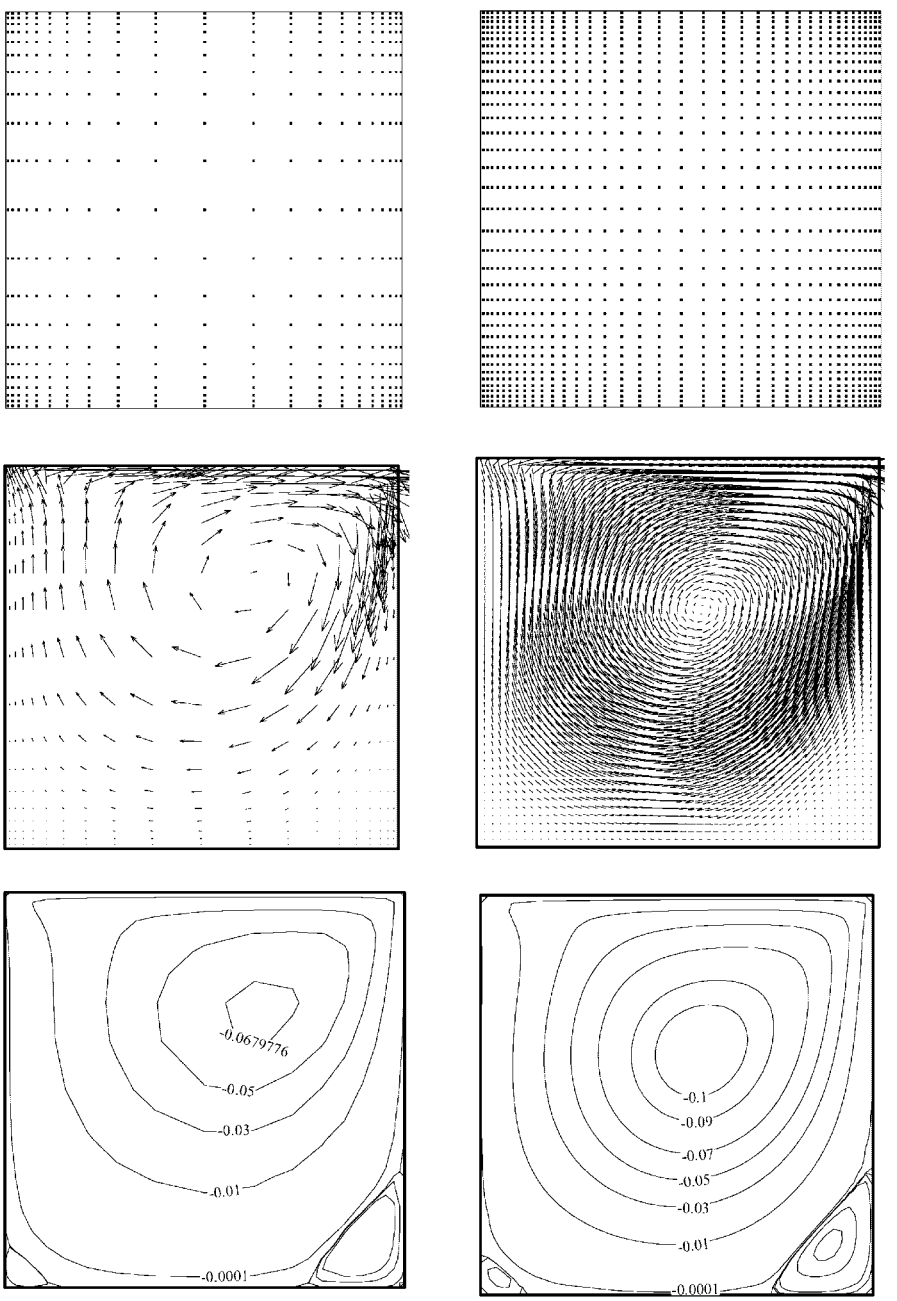

(a) 441 points (b) 2601 points

Figure 5. Comparison of velocity field and streamline for $Re = 400$ and different number of points: (a) and (b) structured points, (c) and (d) unstructured points.

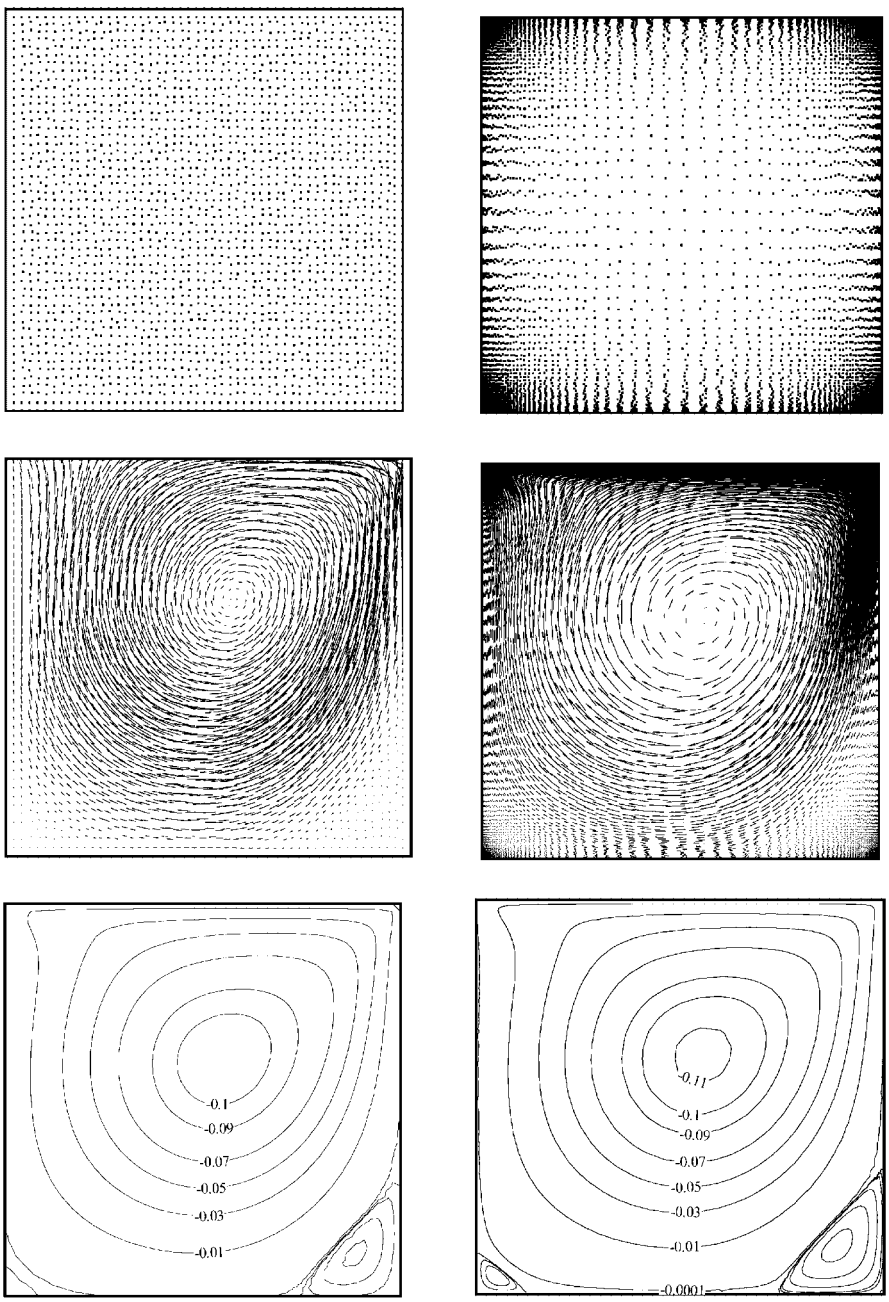

(c) 2601 points (d) 13689 points

Figure 5. *Continued.*

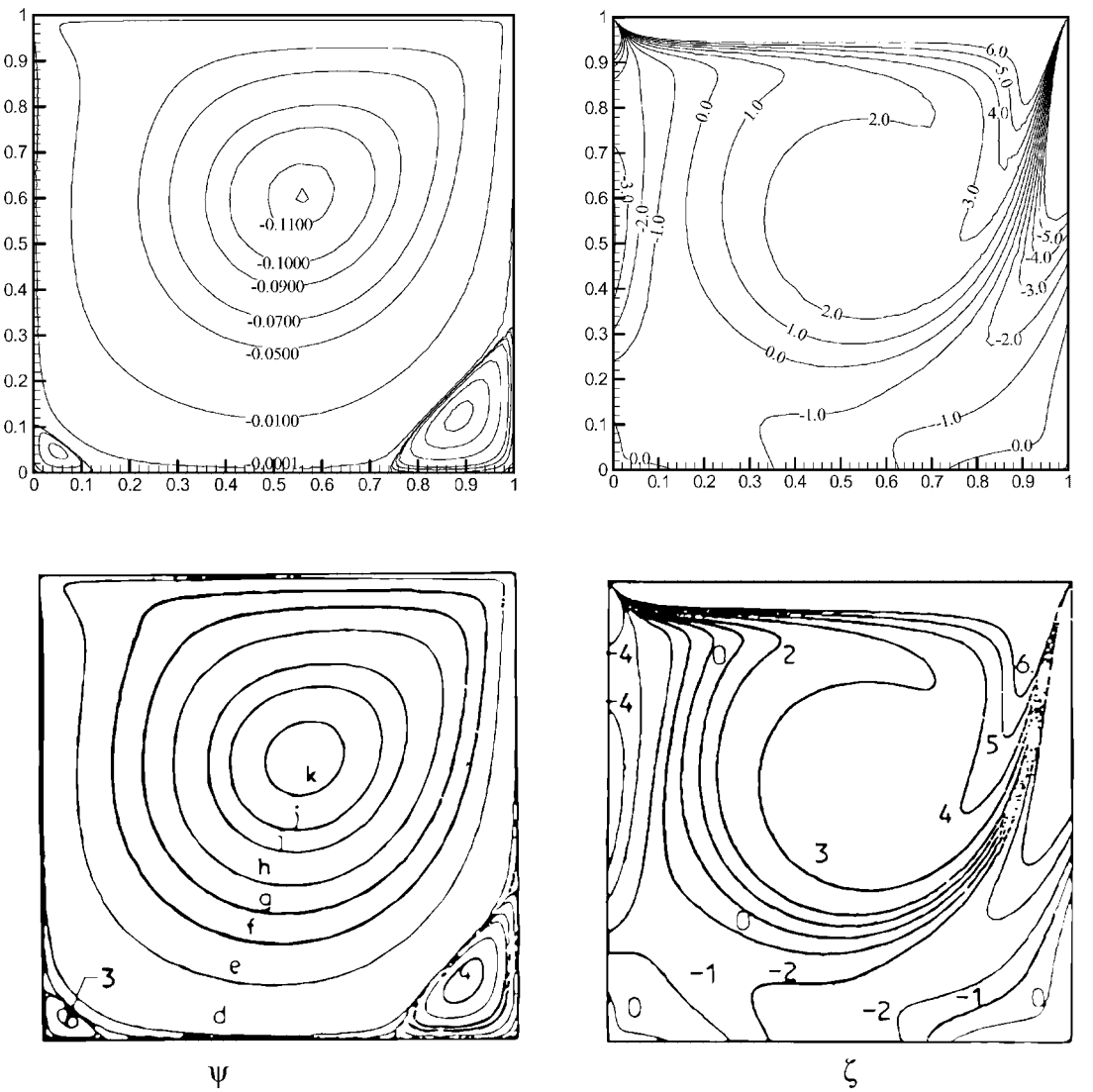

Figure 6. Comparison of the values of streamline and vorticity contours obtained by FPM (upper, 13 689 unstructured points) and by FDM (lower, 129×129 nodes) [15] at $Re = 400$. The values of ψ are d——-0.0001, e——-0.0100, f——-0.0030, g——-0.05, h——-0.07, i——-0.09, j——-0.100, k——-0.110, the value of ζ are 0—0.0, ± 1—± 0.5, ± 2—± 1.0, ± 3—± 1.0, ± 4—± 3.0, ± 5—± 4, ± 6—± 5.0.

$$\psi = y\left(1 - \frac{1}{x^2 + y^2}\right), \quad \zeta = 0 \text{ on } \Gamma_2 \tag{32}$$

where Γ_1 and Γ_2 are the surfaces of the cylinder and the outer boundary far from the cylinder, respectively. The initial vorticity can be approximated from Rayleigh's solution [17].

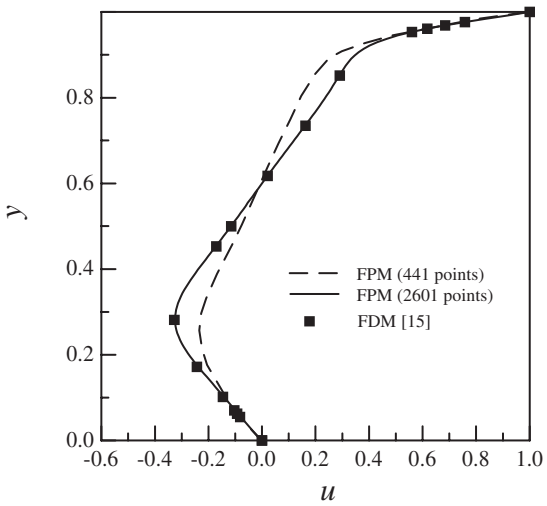

(a) Velocity profiles for u through the geometric center of cavity

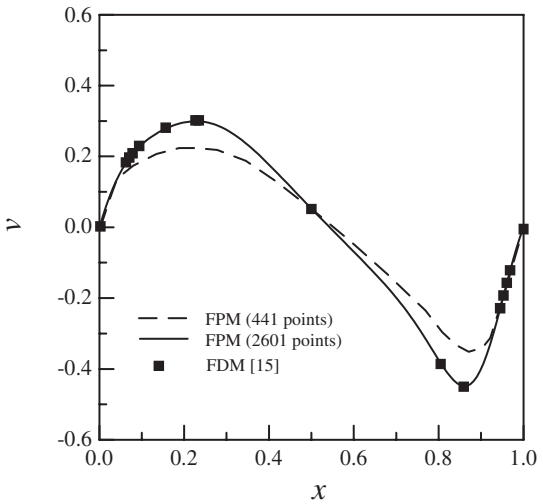

(b) Velocity profiles for v through the geometric center of cavity

Figure 7. Velocity profiles through the geometric centre of cavity at different structured points. Symbols are data from Reference [15].

The initial development of impulsively started flow around a cylinder for $Re=3000$ has been studied numerically and experimentally by some researchers. The present results are compared with the experimental visualization results obtained by Bouard and Coutancea [18], as shown in Figure 9. Both show the elongation with time of the main vortex and the appearance of a secondary vortex of opposite vorticity near the separation point at time $t=3$. The secondary vortex grows in size until it touches the boundary of the main recirculation

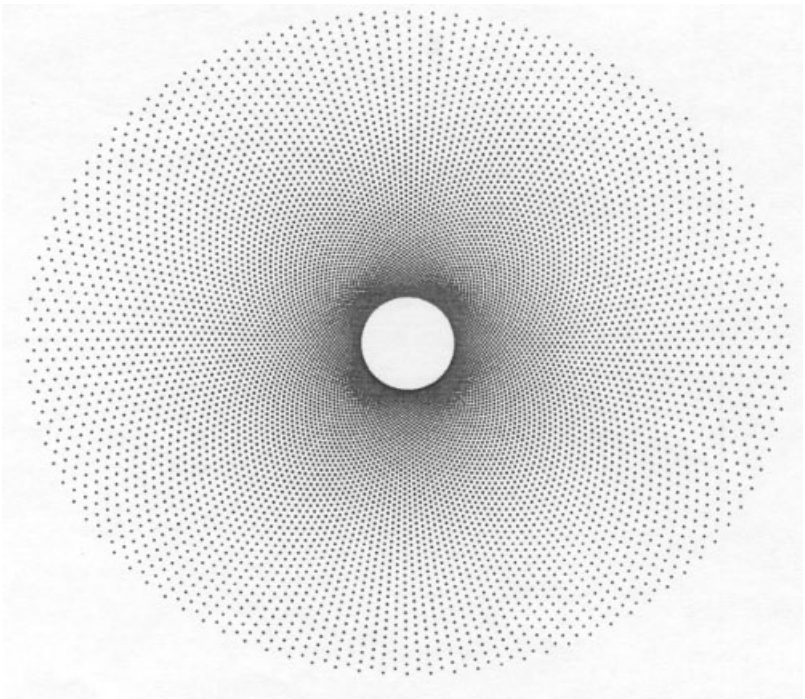

Figure 8. Points distribution for flow past a circular cylinder.

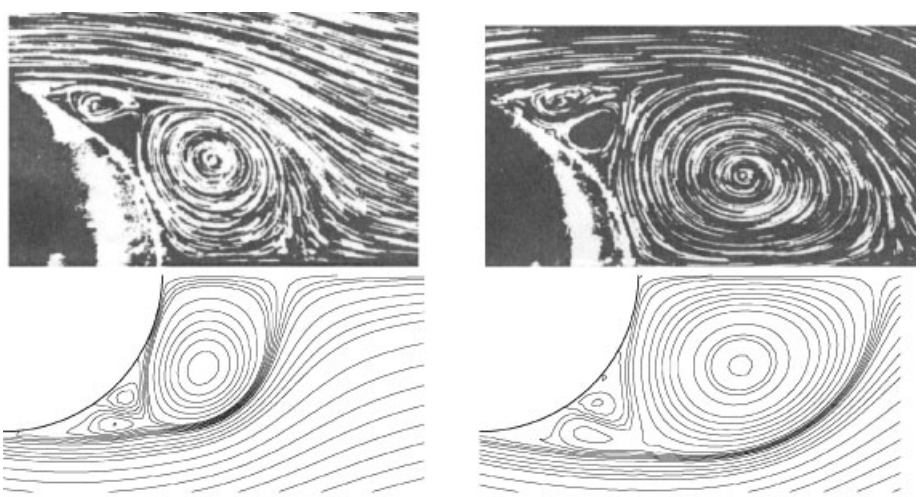

Figure 9. Comparison of experimental flow visualization [17] (upper) with streamlines (lower) by FPM for $Re=3000$ at times (a) $t=3$ and (b) $t=5$.

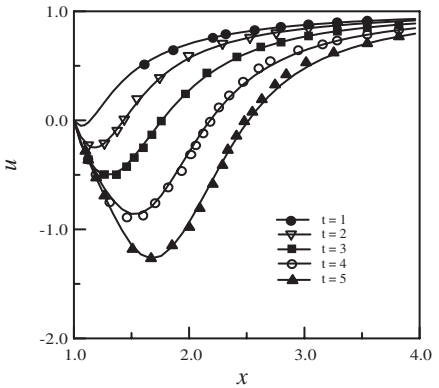

(a) Evolution with time of vertical velocity profiles on the symmetric axis behind the cylinder

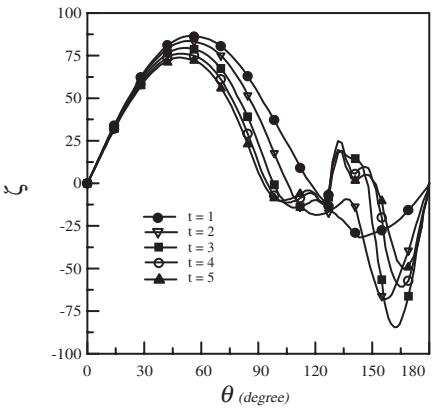

(b) Evolution with time of vorticity distribution on the surface of the cylinder

Figure 10. Comparison of velocity profiles and vorticity distribution on the surface of the cylinder from experimental (symbols), present (solid line) and the finite difference (symbols) results at $Re = 3000$. Symbols are data from References [17, 18].

zone and splits the main vortex into two parts. Two secondary vortices of opposite vorticity emerge in the part near the separation location and constitute the so-called α-phenomenon at $t = 5$ (see Figure 9(b)).

Figure 10 shows a comparison of the present with experimental and numerical results for the velocity profiles and surface vorticity. The evolution with time of vertical velocity on the symmetric axis behind the cylinder is compared with the experimental results of Bouard and Coutanceau [18] at the same Reynolds number. The present results as shown in Figure 10(a) is in good agreement with the experimental results. A comparison of the time evolution of vorticity distribution over the surface of the cylinder with the numerical results of Ta and Bouard [19] is shown in Figure 10(b). It is found that the present results are also in good agreement with their results during the early stage of the flow. Furthermore, whenever comparison is possible, it is found that the results of the present computations on flow past

a cylinder are found to be in good agreement with the experimental and numerical results obtained by other investigators.

4. CONCLUDING REMARKS

The numerical results show that the present method is capable of satisfactorily predicting the flow characteristics in the vicinity of the body surface, such as flow separation. The main characteristics of the present method are summarized as follows:

The algorithm is simple, and it is parallel in nature due to the locality of point information, so it is well suited to massively parallel computing. The extension of the present method to three-dimensional problems is straightforward.

It is effective to handle the non-linear convection terms by means of the upwind-dominated 6-point scheme, and flexible to handles complex boundary conditions and complex properties of fluid system.

If one is interested in only global property, such as flow pattern, a relatively coarse point distribution should be adopted. If the resolution of local properties is also of interest, a finer point distribution will be necessary. The computation time grows with the increase of the number of points. But for structured point distribution, $\delta < 1.1$, when the points are greater than a certain number the error approaches an asymptotic value.

REFERENCES

1. Perrone N, Kao R. A general finite difference method for arbitrary meshes. *Computers & Structures* 1975; **5**:45–58.
2. Liszka T, Orkisz J. The finite difference method at arbitrary irregular grids and its application in applied mechanics. *Computers & Structures* 1980; **11**:83–95.
3. Liszka T. An interpolation method for an irregular net of nodes. *International Journal for Numerical Methods in Engineering* 1984; **20**:1599–1612.
4. Gingold RA, Moraghan JJ. Smooth particle hydrodynamics: theory and applications to non-spherical stars. *Royal Astronomical Society, Monthly* Notices. 1977; **181**:375–389.
5. Lucy LB. A numerical approach to the testing of fusion process. *Astronomical Journal* 1977; **88**:1013–1024.
6. Libersky LD, Petschek AG. Smooth particle hydrodynamics with strength of materials. *Advances in the Free Lagrange Method*, Lecture Notes in Physics, Vol. 395, Trease HE, Fritts MJ, Crowley WP (eds.). Springer: Berlin and New York, 1990; 248–257.
7. Belytschko T, Lu YY, Gu L. Element-free Galerkin method. *International Journal for Numerical Methods in Engineering* 1994; **37**:229–256.
8. Liu WK, Jun S, Belytschko T. Reproducing Kernel particle method. *International Journal for Numerical Methods in Fluids* 1995; **20**:1081–1106.
9. Liu WK, Chen Y. Wavelet and multiple scale producing Kernel particle method. *International Journal for Numerical Methods in Fluids* 1995; **21**:901–931.
10. Liu GR, Yang KY. A penalty method for enforcing essential boundary conditions in element free Galerkin method. *Proceedings of the 3rd HPC Asia'98*, Singapore, 1998; 715–721.
11. Liu GR. A point assembly method for stress analysis for solids. *The 3rd International Symposium on Impact Engineering*, December, U.K., 1998; 475–480.
12. Liu GR, Yang KY. A new meshless method for stress analysis for solids and structures. *The 4th Asia–Pacific Conference on Computational Mechanics for the next Millennium*, December, Singapore, 1999; 973–984.
13. Onate E, Idelsohn S, Zienkiewicz OC, Taylor RL. A finite point method in computational mechanics applications to convective transport and fluid flow *International Journal for Numerical Methods in Engineering* 1996; **39**:3839–3866.
14. Duarte CAM. A review some meshless methods to solve partial differential equations. *TICAM Report* 95-06, The University of Texas, Austin, May 1995.
15. Ghia U, Ghia KN, Shin CT. High-Re solution for incompressible flow using the Navier–Stokes equations and a multigrid method. *Journal of Computational Physics* 1982; **48**:387–411.

16. Chen S, Doolen G, Cogley AC. Simulation of cavity flow by the Lattice Boltzmann Method. *Journal of Computational Physics* 1995; **118**:329–347.
17. Telionis DP. *Unsteady Viscous Flows*. Springer: New York, 1981.
18. Bouard R, Coutancea M. The early stage development of the wake behind an impulsively started cylinder for $40 < Re < 10^4$. *Journal of Fluid Mechanics* 1980; **101**:583–607.
19. Ta Phuoc Loc, Bouard R. Numerical solution of the early stage of the unsteady viscous flow around a circular cylinder: a comparison with experimental visualization and measurements. *Journal of Fluid Mechanics* 1985; **160**:93–117.

